ANALYSIS OF LIQUID IMPACT PHENOMENA AFFECTING RAIN EROSION FAILURE IN WIND TURBINE BLADES. A VISCOELASTIC PARAMETRIC STUDY

Claudia Germoso[1, a)], Fernando Sánchez[2, b) *], Luis Domenech[2, c)], Enrique Cortés[3, d)], Antonio Falcó[2, e)], Francisco Chinesta[4, f)]

[1] Instituto Tecnológico de Santo Domingo, INTEC, Av. de Los Próceres 49, 10602 Santo Domingo, Rep. Dominicana,
Email: [a)] claudia.germoso@intec.edu.do
[2] ESI Chair at CEU-UCH, Departamento de Matemáticas, Física y Ciencias Tecnológicas, Universidad Cardenal Herrera-CEU, CEU Universities, 46115 Moncada-Valencia, Spain ;
Email: [b)] * Corresponding author: fernando.sanchez@uchceu.es,
[c)] luis.domenech@uchceu.es, [e)] afalco@uchceu.es
[3] AEROX Advanced Polymers, 46185 Pobla Vallbona-Valencia, Spain,
Email: [d)] ecortes@aerox.es
[4] ESI Chair at PIMM, ENSAM ParisTech, 151 Boulevard de l'Hopital, 75013 Paris, France,
Email: [f)] Francisco.Chinesta@ensam.eu

Keywords: Wind turbine blades; rain erosion; coatings; leading edge protection; computational modelling; PGD-Proper Generalized Decomposition

Abstract
Rain erosion damage, caused by repeated droplet impact on wind turbine blades, is a major cause for concern, even more so at offshore locations with larger blades and higher tip speeds. Analytical and numerical models are commonly used to relate top coating lifetime prediction and to identify suitable coating and composite substrate combinations based on their potential stress reduction on the surface and interface. The numerical models usually applied for the analysis of rain erosion impact are limited to a linear elastic response of the polymer subjected to drop impact loads. It is important to note that polymeric materials response depend on temperature and also on stress and strain rates. If these parameters are not incorporated in the mechanical modeling, the predicted stresses of the coating behavior under impingement may wrongly consider the material capabilities. In order to develop an appropriate multi-parametric approach based on the viscoelastic material characterization, it is also necessary to consider a computational tool that allows one to design and validate the proposed modelling. In this research, a tensional analysis of candidate materials in the temporal and frequency domain is developed. This work proposes an integral numerical model that links the calculation of stress with the service conditions (temperature, rainfall intensity, droplet size, impact speed, impact frequency) treated as parameters and considering the construction of the pulsed material response for the computational modeling.

1. Introduction

One of the major sector trend to improve efficiency is based on increasing the Wind turbines rotor diameters to capture more wind energy. However, this increase in diameter involves an escalation in the tip speed. When considering the impact force of rain droplets, hailstones and other particulates on the blade leading edge, the tip speed is a key contributor to erosion damage on the surface, see Fig. 1 (a). Industrial processes state that LEP systems can be outlined as a multi-layered system, where some manufacturers include a putty layer between the composite laminate and the coating, see Fig. 1 (b). It

also can be included a primer layer under the coating and over the filler to improve adhesion mainly on service conditions.

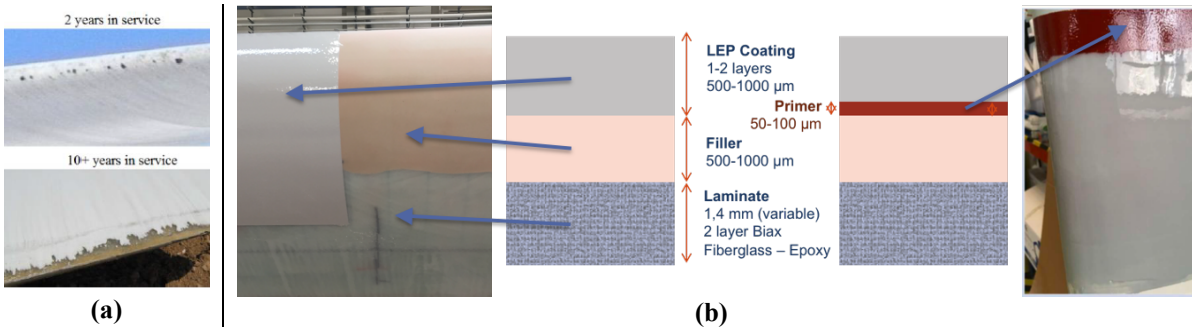

Figure 1. (a) Erosion Damage (b) Leading Edge Protection (LEP) system configuration [3]

Analytical and numerical models are commonly used to identify suitable coating and composite substrate combinations based on their potential stress reduction on the surface and interfaces under droplet impingement and also for lifetime erosion damage prediction. The numerical models known are limited to a linear elastic response of the polymer subjected to drop impact loads and not consider the interfaces contact failure,[1],[2]. In this research, the polymeric mechanical models are used within a novel multi-parametric approach based on the viscoelastic material characterization that links the calculation of stress-strain behaviour with the service conditions conditions (temperature, rainfall intensity, droplet size, impact speed, impact frequency). A numerical tool to quantify the potential stress impact reduction when varying the material and the geometrical parameters of the LEP system configuration has been developed.

2. Mechanical Modelling

2.1. Liquid Impact Phenomena and erosion failure

An essential aspect of understanding how erosion is caused on the coating material is to consider the physical effects initiated by the impingement of the liquid droplets upon the material surface. The analysis of erosion damage caused by rain droplets shows that the damage is in fact a dynamic event resulting in the propagation of shock waves, see Fig. 2. As the water droplet impinges on the surface at a normal angle, two wave fronts are created with the longitudinal compressional normal stress wave preceding a transverse shear wave. The impact gives rise to a third wave due to the water droplet deformation itself, called the Rayleigh wave, which is confined to the surface of the target [2]. The pressure generated on impact can be referred to as the water-hammer pressure and the magnitude varies depending on the acoustic properties of the target material and the liquid [1]:

$$P_{water-hammer} = V\left(\frac{\prod_{i=1}^{2} Z_i}{\sum_{i=1}^{2} Z_i}\right) \quad ; \quad Z_i = \rho_i C_i \quad ; \quad C_i = \sqrt{\frac{E_i}{\rho_i}} \tag{1}$$

Where V is the impact velocity, Z denotes dynamical impedance, ρ the density, C the shock wave velocity, E the elastic modulus, and the indices i=1, 2 denote the properties of the liquid and solid respectively. The duration of the impact pressure on the surface is directly related with the radius of the droplet. The maximum pressure does not occur at the epicentre of impact at the instant of first contact but at some delayed time in a ring around the midpoint at a location where the contact circle edge is reached by the initial shockwave generated by the impact. Maximum shear stresses are observed on these radial locations and have a very short duration compared with the central compressional pressures. The erosion failure can be initiated by a local imbalance of tensile and shear stresses in regions that may be outside the direct impact area. The post-impact shock wave also propagates through the LEP multi-

layer system materials and depends on the elastic and viscoelastic responses and the interactions between layers [3]. Stress reflections oscillate repeatedly through the coating and substrate structure until dampened out by the materials' properties.

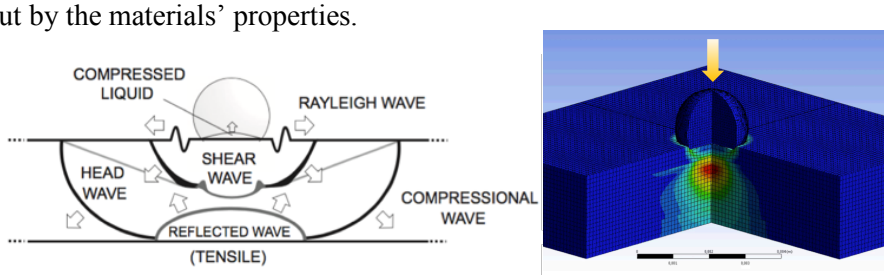

(**a**) (**b**)

Figure 2. (**a**) Illustrates the three waves that develop following the droplet collision [2]; (**b**) Numerical simulation of a droplet impact on a multi-layer LEP configuration.

2.2. Leading Edge Protection Viscoelastic Modelling with Havriliak-Negami Model

The waterdrop impacts on rotor blades are highly transient events that introduce a very high-rate transient pressure buildup. The LEP viscoelastic material experiences a very rapidly increasing stress field that leads to a distortion and a subsequent strain relaxation. This transient material behaviour can be obtained from the frequency response data (DMTA) and transforming the data from the frequency to the time domain can be required. A well known method for the modeling of polymeric relaxation behaviour with respect to dielectric and/or mechanical data in the frequency domain is the *Havriliak-Negami Model* [4]. It states that

$$E^* = E_\infty + (E_0 - E_\infty) \times \frac{1}{[1 + (i\omega\tau)^\alpha]^\beta} \quad ; \quad E^* = E' - iE'' \tag{2}$$

where E* is the complex modulus, E_∞ is the unrelaxed or glassy modulus, E_0 is the relaxed rubbery modulus, i is the characteristic complex number $\sqrt{-1}$, ω is the angular frequency (where $\omega = 2\pi f$), τ is the relaxation time and is temperature dependent. As complex modulus (E*) data from dynamic mechanical spectroscopy can be resolved by complex analysis into its in-phase, storage (E′) modulus and out-of-phase, loss (E″) modulus. Other parameters α and β are shape characteristics of the fitted curve where $0 < \alpha, \beta \leq 1$, where α influences the width and β influences the asymmetry of the curve. E_∞ can be estimated from the values of E (modulus) data at low temperatures, high frequencies ($\omega \to \infty$) and E_0 can be estimated from E (modulus) data at high temperatures and low frequencies ($\omega \to 0$), as it can be seen in Fig. 3.

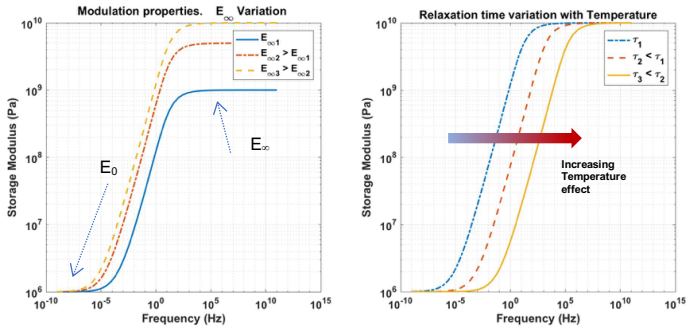

Figure 3. (a) H-N model. Storage Modulus variation with Frequency. E_∞ unrelaxed modulus variation **(b)** Relaxation Time dependence on Temperature

2.3. Elasticity problem. In plane out of plane separated representation of a 3D multilayered plate.

Authors have recently proposed a powerful new discretization technique based on the use of separated representations called Proper Generalized Decomposition (PGD), which demonstrates their ability to solve multidimensional models. This technique works by building separated representations of the solution, in that way, the complexity scales of the solution are linear with the dimension of the space in which the model is defined, instead of exponentially growing complexity of the mesh, based on commons discretization techniques. The PGD methods allows the efficient solution of the models to be defined in multidimensional spaces such as those found in quantum chemistry, kinetic theory descriptions of complex fluids, genetics, etc. For problems where the norms are defined in space and time, we add new coordinates resulting numerous possibilities.
The method consists of introducing model parameters as extra coordinates, in the same way that time and space were originally defined in the problem. The problem is then solved once for all the coordinates allowing circumvent the so-called curse of dimensionality. The interested reader can also refer to the recent reviews [5], [6],[7],[8].

In what follows we describe the construction of the parametric solutions within the Proper Generalized Decomposition framework. We considered the in-plane-out-of-plane decomposition for solving 3D problems in plates. In [10] is considered the in-plane-out-of-plane decomposition for solving 3D elastic problems in plate geometries. The separated representation of the displacement field $U = (u, v, w)$ reads:

$$U(x,y,z) = \begin{pmatrix} u(x,y,z) \\ v(x,y,z) \\ w(x,y,z) \end{pmatrix} = \sum_{i=1}^{N} \begin{pmatrix} X_u^i(x,y) \cdot Z_u^i(z) \\ X_v^i(x,y) \cdot Z_v^i(z) \\ X_w^i(x,y) \cdot Z_w^i(z) \end{pmatrix} = \sum_{i=1}^{N} \mathbf{X}^i(x,y) \circ \mathbf{Z}^i(z) \tag{3}$$

where "∘"stands for Hadamard (component –wise) product. Vectors $\mathbf{X}^i$ are the functions in the plane (x, y) and $\mathbf{Z^i}$ are the functions involving the thickness (z). Is important to know that the above functions are not known a priori but are calculated by the same method by introducing the separated representation of the solution in the weak formulation of the problem resulting in a nonlinear problem. This implies that iterations are needed at each enrichment step.

The weak formulation of the dynamics elasticity problem in a body Ω writes as follows:

$$-\int_{\Omega} U^{*t} \rho \omega^2 \; U \, d\Omega + \int_{\Omega} \varepsilon^{*t} D \varepsilon \, d\Omega = \int_{\Omega} U^{*t} F \, d\Omega \tag{4}$$

where the domain $\Omega = \Omega_{xy}$ x Ω_z with $(x, y) \in \Omega_{xy}$ and $z \in \Omega_z$. The linear elastic isotropic material is given by the generalized 6x6 Hooke tensor:

$$D = \begin{bmatrix} \lambda+2\mu & \lambda & \lambda & 0 & 0 & 0 \\ \lambda & \lambda+2\mu & \lambda & 0 & 0 & 0 \\ \lambda & \lambda & \lambda+2\mu & 0 & 0 & 0 \\ 0 & 0 & 0 & \mu & 0 & 0 \\ 0 & 0 & 0 & 0 & \mu & 0 \\ 0 & 0 & 0 & 0 & 0 & \mu \end{bmatrix}; \quad \lambda = \frac{\nu E}{(1+\nu)(1-2\nu)} \quad ; \quad \mu = \frac{E}{2(1+\nu)} \tag{5}$$

where E is the young modulus, ν the Poisson coeficient, ρ the density and F is the volumetric body forces. We use the following definitions to the strain vector components:

$$\varepsilon = \begin{vmatrix} \varepsilon_x \\ \varepsilon_y \\ \varepsilon_z \\ \gamma_{xy} \\ \gamma_{xz} \\ \gamma_{yz} \end{vmatrix} \quad \begin{aligned} \varepsilon_x &= \frac{\partial u}{\partial x} = \sum_{i=1}^{n-1} \frac{\partial X_u^i}{\partial x} Z_u^i & \gamma_{xy} &= \frac{\partial u}{\partial y} + \frac{\partial v}{\partial x} = \sum_{i=1}^{n-1} \frac{\partial X_u^i}{\partial y} Z_u^i + \frac{\partial X_v^i}{\partial x} Z_v^i \\ \varepsilon_y &= \frac{\partial v}{\partial y} = \sum_{i=1}^{n-1} \frac{\partial X_v^i}{\partial y} Z_v^i & \gamma_{xz} &= \frac{\partial u}{\partial z} + \frac{\partial w}{\partial x} = \sum_{i=1}^{n-1} X_u^i \frac{\partial Z_u^i}{\partial z} + \frac{\partial X_w^i}{\partial x} Z_w^i \\ \varepsilon_z &= \frac{\partial w}{\partial z} = \sum_{i=1}^{n-1} X_w^i \frac{\partial Z_w^i}{\partial z} & \gamma_{yz} &= \frac{\partial v}{\partial z} + \frac{\partial w}{\partial y} = \sum_{i=1}^{n-1} X_v^i \frac{\partial Z_v^i}{\partial z} + \frac{\partial X_w^i}{\partial y} Z_w^i \end{aligned} \tag{6}$$

Supposing that U^{n-1} to be known, we focus on the solution enrichment related to the computation of the next functional product $X^n(x,y)$ and $Z^n(z)$, according to:

$$U(x,y,z) = U^{n-1}(x,y,z) + \begin{pmatrix} X_u^n(x,y) \cdot Z_u^n(z) \\ X_v^n(x,y) \cdot Z_v^n(z) \\ X_w^n(x,y) \cdot Z_w^n(z) \end{pmatrix}$$

or

$$U(x,y,z) = U^{n-1}(x,y,z) + \mathbf{X}^n(x,y) \circ \mathbf{Z}^n(z) \tag{7}$$

The test function U^*reads

$$U^*(x,y,z) = \begin{pmatrix} u^*(x,y,z) \\ v^*(x,y,z) \\ w^*(x,y,z) \end{pmatrix} = \begin{pmatrix} X_u^*(x,y) \cdot Z_u^n(z) + X_u^n(x,y) \cdot Z_u^*(z) \\ X_v^*(x,y) \cdot Z_v^n(z) + X_v^n(x,y) \cdot Z_v^*(z) \\ X_w^*(x,y) \cdot Z_w^n(z) + X_w^n(x,y) \cdot Z_w^*(z) \end{pmatrix} \tag{8}$$

Finally, introducing Eq. (3) into Eq.(6) and Eq. (8) into the Eq. (4) the resulting weak form reads now

$$\begin{aligned} -\int_\Omega \left[u^* \rho\omega^2 u + v^* \rho\omega^2 v + w^* \rho\omega^2 w\right] d\Omega \\ + \int_\Omega \left[\varepsilon_x^* \theta\varepsilon_x + \varepsilon_y^* \lambda\, \varepsilon_x + \varepsilon_z^* \lambda\, \varepsilon_x + \varepsilon_x^* \lambda\, \varepsilon_y + \varepsilon_y^* \theta\varepsilon_y + \varepsilon_z^* \lambda\, \varepsilon_y + \varepsilon_x^* \lambda\, \varepsilon_z \right. \\ \left. + \varepsilon_y^* \lambda\, \varepsilon_z + \varepsilon_z^* \theta\varepsilon_z + \gamma_{xy}^* \mu\, \gamma_{xy} + \gamma_{xz}^* \mu\, \gamma_{xz} + \gamma_{yz}^* \mu\, \gamma_{yz}\right] d\Omega \end{aligned} \tag{9}$$

where $\theta = \lambda + 2\mu$. The introduction of Eq. (7) into to (9) results a non-linear problem. We proceed by considering the simplest linearization strategy, an alternated directions fixed point algorithm, that proceed by assuming sequentially that $\mathbf{Z}^{n,p-1}(z)$ is known of the previously iteration, and proceed to compute $\mathbf{X}^{n,p}(x,y)$. Finally with $\mathbf{X}^{n,p}(x,y)$ is computed $\mathbf{Z}^{n,p}(z)$. The process is repeated in a suitable fixed-point iteration scheme, until reaching convergence, where the results will be the new products $\mathbf{X}^n(x,y)$ and $\mathbf{Z}^n(z)$. The enrichment stop when the model residual become small enough.
First, we assume $\mathbf{Z}^n(z)$ to be known from the previous iteration, in this case the test function is $U^* = \mathbf{X}^*(x,y) \circ \mathbf{Z}^n(z)$. Introducing the separated representation of the solution at iteration n (Eq. 7) and the test function into Eq. (6) and then integrating in Ω_{xy}, the resulting 2D equation can be interpreted as the weak formulation in which we can obtain the unknown function $\mathbf{X}^n(x,y)$, that can be solved by using any suitable discretization techniques.

Finally, with the new value of $\mathbf{X}^n(x,y)$, the test function is chosen equal to $U^* = \mathbf{X}^n(x,y) \circ \mathbf{Z}^*(z)$. By introducing the (Eq. 7) and the test function into the weak formulation (Eq. 9) and integrating in Ω_z, we obtain the resulting 1D weighted residual form that can be solved by using any discretization technique to obtain the unknown function $\mathbf{Z}^n(z)$.

2.4. Proper generalized decomposition-based parametric solutions. Case application

In this section, we describe the parametric solutions within the Proper Generalized Decomposition framework for a given application as an example. The model set up used in the study case is depicted in Fig. 4 (a) showing a configuration of 5 layers where the material parameters and thicknesses can be considered as parameters in the analysis. The droplet impact is modelled as step function defined by Water-Hammer pressure on Eq.(1) and its duration is directly related with the droplet size [1].

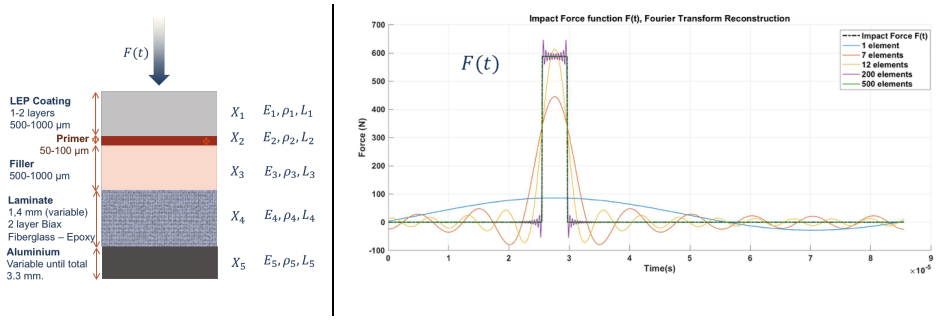

(a) **(b)**

Figure 4. (a) Model set up. **(b)** Impact force step wise definition and Fourier Reconstruction.

The plate is assumed composed of $\mathcal{L}$ layers $\delta_i, i = 1, \dots, \mathcal{L}$. Each layer is identified from its characteristic function $\chi_i(z),\ i\ = 1,\cdots,\mathcal{L}$, defined as

$$\chi_i(z) = \begin{cases} 1 & \text{if} \quad z \in \delta_i \\ 0 & \text{if} \quad z \notin \delta_i \end{cases}$$

with $\mathcal{L} = 5$ for this case. First layer mechanical modulus depend on the frequency and relaxation time (τ), in this case we have a two-dimensional field $E_1^*(\omega, \tau)$ and the dimensions (ω, τ) are considered as coordinate of the model, we can use the PGD for calculating the n-term separated approximation of the given function $E_1^*(\omega, \tau)$, given by

$$E_1^*(\omega, \tau) = \sum_{j=1}^{k} \mathcal{M}_j(\omega) \mathrm{N}_j(\tau)$$

We shall see in [7], [9] how to obtain a separated representation of $E_1^*(\omega, \tau)$. The material parameters related with the first layer now can read,

$$\lambda_1 = \frac{\nu\left(\sum_{j=1}^{k} \mathcal{M}_j \mathrm{N}_j\right)}{(1+\nu)(1-2\nu)} \quad ; \qquad \mu_1 = \frac{\left(\sum_{j=1}^{k} \mathcal{M}_j \mathrm{N}_j\right)}{2(1+\nu)}$$

the resulting weak form (Eq. 9), reads

$$\begin{aligned} -\int_\Omega \big[& u^*(\rho_1\chi_1 + \rho_2\chi_2 + \cdots + \rho_\mathcal{L}\chi_\mathcal{L})\ \omega^2 u + v^*(\rho_1\chi_1 + \rho_2\chi_2 + \cdots + \rho_\mathcal{L}\chi_\mathcal{L})\ \omega^2 v \\ & + w^*(\rho_1\chi_1 + \rho_2\chi_2 + \cdots + \rho_\mathcal{L}\chi_\mathcal{L})\ \omega^2 w \big]\ d\Omega \\ & + \int_\Omega \left[\frac{\partial u^*}{\partial x}(\theta_1\chi_1 + \theta_2\chi_2 + \cdots + \theta_\mathcal{L}\chi_\mathcal{L})\ \frac{\partial u}{\partial x} + \frac{\partial v^*}{\partial y}(\lambda_1\chi_1 + \lambda_2\chi_2 + \cdots + \lambda_\mathcal{L}\chi_\mathcal{L})\ \frac{\partial u}{\partial x} \right. \\ & \left. + \frac{\partial w^*}{\partial z}(\lambda_1\chi_1 + \lambda_2\chi_2 + \cdots + \lambda_\mathcal{L}\chi_\mathcal{L})\ \frac{\partial u}{\partial x} + \cdots \right] d\Omega \end{aligned}$$

where the domain $\Omega = \Omega_{xy}\ \mathrm{x}\ \Omega_z\ \mathrm{x}\ \Omega_\omega \mathrm{x}\ \Omega_{\mathrm{E}_0} \mathrm{x}\ \Omega_{E_\infty} \mathrm{x}\ \Omega_\tau$. Now $\lambda_2 \dots \lambda_\mathcal{L}$ and $\mu_2 \dots \mu_\mathcal{L}$ are given by Eq. 5

with the properties of each layer. The PGD solution in the separated form can be implemented as

$$u(x,y,z,\omega,E_0,E_\infty,\tau) \approx \sum_{i=1}^{N} \mathbf{X}^i(x,y) \circ \mathbf{Z}^i(z) \circ \mathbf{W}^i(\omega) \circ \mathbf{E_0}^i(E_0) \circ \mathbf{E_1}^i(E_\infty) \circ \mathbf{T}^i(\tau) \qquad (10)$$

3. Results

This sections shows the numerical capabilities of the numerical algorithm for computing a fine enough solution while circumventing the difficulties related to the excessive degrees of freedom of fully 3D mesh-based discretization, we took advantage of in-plane-out-of-plane separated representations within the Proper Generalized Decomposition (PGD) framework that permitted capturing details of the mechanical fields along the laminate thickness.

Fig.5 (a) illustrates Maximum Z-Stress evolution with the impedance computation from Eq. (1) where the storage modulus is assumed E_∞ for a parameter range on the frequencies of interest. The values are computed for Layer 1 (in blue), Layer 2 (in orange) and their interface (in green) on the central point of impact. It is very interesting to observe that when the impedance value of Layer 1 is higher than a given constant value of Layer 2 (in red), the Maximum Z-Stress occurs on the surface of Layer 1, and when the impedance is lower than this threshold value, it occurs at the interface. This result is very usefull for the modelling of suitable materials combinations to be used as a multilayer scheme, and allows one to match the acoustic material properties in orther to minimize the stress reflections and transmisions through the laminate thickness. This result is less apparent when considering the shear stress calculations at a radial distance of the impact location as it can be observed Fig.5 (b) showing the computational tool potential in terms of LEP material candidate selection and properties modulation.

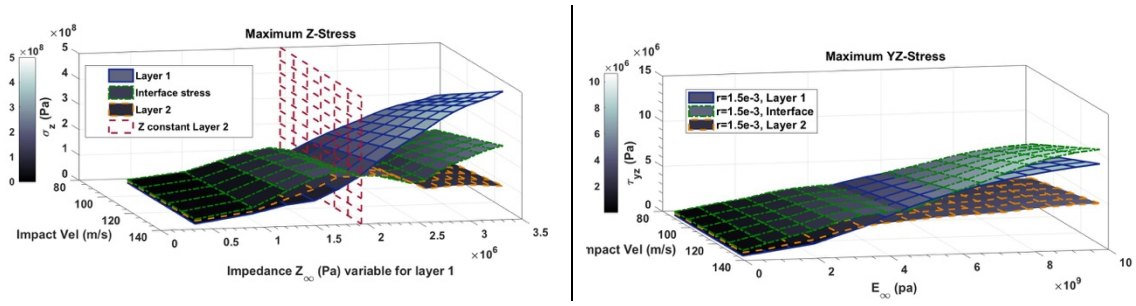

(a) **(b)**

Figure 5. (a) Maximum Compresional-Tensile Stress vs Impedance and Impact velocity as parameters **(b)** Maximum Shear Stress vs E_∞ unrelaxed modulus from Eq. (2) and Impact velocity as parameters.

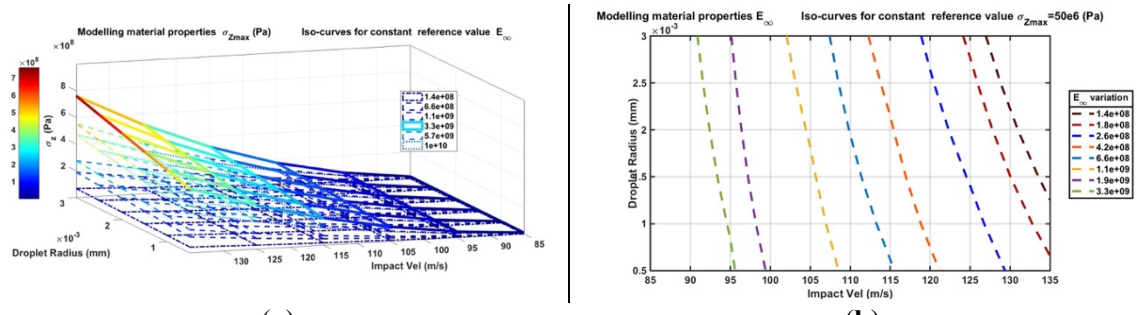

(a) **(b)**

Figure 6. (a) Maximum Compresional-Tensile Stress for E_∞ unrelaxed modulus as material parameter. **(b)** Iso-curves of E_∞ unrelaxed modulus for a reference value of the Compresional-Tensile Stress

Other field of application is proposed when considering to analyze a proper material for the LEP system for a given blade diameter. Since the impact velocity depends on the blade size it is remarkable to observe in Fig. 6 how the E_∞ value of a given material candidate is able or not to achieve a threshold Maximum Z-Stress. This is very interesting to account since it has been computed parmetrically for any rain droplet size and impact velocity.

4. Conclusions

This research presents a versatile multi-parametric approach that accounts for the viscoelastic material characterization in the analysis of the rain erosion impact phenomena on leading edge Protection systems of wind turbine blades. A tensional analysis of candidate top coating materials in the temporal and frequency domain is developed in an integral numerical model that links the calculation of stress with the service conditions (temperature, rainfall intensity, droplet size, impact speed, impact frequency) treated as parameters and considering the construction of the pulsed material response for the computational modeling. The tool can be used to identify suitable coating and composite substrate combinations based on their potential stress reduction on the surface and interface layers. The numerical algorithm capabilities for computing a fine enough 3D solution is based on the use of in-plane-out-of-plane separated representations within the Proper Generalized Decomposition (PGD) framework that permitted capturing details of the mechanical fields along the laminate thickness. Further work is on development for the complete material parametrization and geometrical configurations.

Acknowledgments

This research has been partially funded by the DEMOWIND-2 Project 'Offshore Demonstration Blade (ODB) Funded by MINECO with reference PCIN-069-2017 and by the ESI-Group Chair at CEU-UCH.

References

[1] Springer, G.S. Erosion by Liquid Impact; *Scripta Technica Publishing Co.* 1976.
[2] Gohardani, O. Impact of erosion testing aspects on current and future flight conditions. *Prog. Aerosp. Sci. 2011, 47, 280–303*
[3] E.Cortés, F.Sánchez, A.O'Carroll, B.Madramany, M.Hardiman,T.M.Young; On the material characterization of wind turbine blade coatings: Effect of the interphase adhesion on rain erosion performance, *Materials; September 2017, Vol 10, 1146, doi:10.3390/ma10101146.*
[4] J.P. Szabo, I.A. Keough, Method for analysis of dynamic mechanical thermal analysis data using the Havriliak-Negami model, *Thermochimica Acta 392-393 (2002) 1-12*
[5] F. Chinesta, A. Ammar, E. Cueto. Recent advances and new challenges in the use of the Proper Generalized Decomposition for solving multidimensional models. *Archives of Computational Methods in Engineering, 17/4, 327-350, 2010.*
[6] F. Chinesta, A. Leygue, F. Bordeu, J.V. Aguado, E. Cueto, D. Gonzalez, I. Alfaro. Parametric PGD based computational vademecum for e_cient design, optimization and control. *Archives of Computational Methods in Engineering, 20/1, 31-59, 2013.*
[7] F. Chinesta, R. Keunings, A. Leygue. The Proper Generalized Decomposition for advanced numerical simulations. *A primer, Springerbriefs, Springer, 2014.*
[8] E. Pruliere, F. Chinesta, A. Ammar. On the deterministic solution of multidimensional parametric models using the Proper Generalized Decomposition. *Mathematics and Computers in Simulation, 81(4), 791-810. 2010.*
[9] C. Germoso. Real-Time Dynamic PGD Calculation of Non-Linear Soil Behavior. 2016.
[10] B. Bognet, F. Bordeu, F. Chinesta, A. Leygue and A. Poitou. Advanced simulation of models defined in plate geometries: 3D solutions with 2D computational complexity. *Computer Methods in Applied Mechanics and Engineering, 201, 1-12. 2012*